RESEARCH ARTICLE

TRK xDFG Mutations Trigger a Sensitivity Switch from Type I to II Kinase Inhibitors

Emiliano Cocco[1,2], Ji Eun Lee[3], Srinivasaraghavan Kannan[4], Alison M. Schram[5,6], Helen H. Won[7], Sophie Shifman[1,2], Amanda Kulick[8], Laura Baldino[1,2], Eneda Toska[1], Amaia Arruabarrena-Aristorena[1], Srushti Kittane[1], Fan Wu[1], Yanyan Cai[1], Sabrina Arena[9,10], Benedetta Mussolin[10], Ram Kannan[3], Neil Vasan[1], Alexander N. Gorelick[1,11], Michael F. Berger[1,2,7], Ofra Novoplansky[12], Sankar Jagadeeshan[12], Yi Liao[13], Uwe Rix[13], Sandra Misale[14], Barry S. Taylor[11], Alberto Bardelli[9,10], Jaclyn F. Hechtman[2], David M. Hyman[5,6], Moshe Elkabets[12], Elisa de Stanchina[8], Chandra S. Verma[4,15,16], Andrea Ventura[3], Alexander Drilon[5,6], and Maurizio Scaltriti[1,2]

ABSTRACT

On-target resistance to next-generation TRK inhibitors in TRK fusion–positive cancers is largely uncharacterized. In patients with these tumors, we found that TRK xDFG mutations confer resistance to type I next-generation TRK inhibitors designed to maintain potency against several kinase domain mutations. Computational modeling and biochemical assays showed that TRKA^{G667} and TRKC^{G696} xDFG substitutions reduce drug binding by generating steric hindrance. Concurrently, these mutations stabilize the inactive (DFG-out) conformations of the kinases, thus sensitizing these kinases to type II TRK inhibitors. Consistently, type II inhibitors impede the growth and TRK-mediated signaling of xDFG-mutant isogenic and patient-derived models. Collectively, these data demonstrate that adaptive conformational resistance can be abrogated by shifting kinase engagement modes. Given the prior identification of paralogous xDFG resistance mutations in other oncogene-addicted cancers, these findings provide insights into rational type II drug design by leveraging inhibitor class affinity switching to address recalcitrant resistant alterations.

SIGNIFICANCE: In TRK fusion–positive cancers, TRK xDFG substitutions represent a shared liability for type I TRK inhibitors. In contrast, they represent a potential biomarker of type II TRK inhibitor activity. As all currently available type II agents are multikinase inhibitors, rational drug design should focus on selective type II inhibitor creation.

[1]Human Oncology and Pathogenesis Program, Memorial Sloan Kettering Cancer Center, New York, New York. [2]Department of Pathology, Memorial Sloan Kettering Cancer Center, New York, New York. [3]Cancer Biology and Genetics Program, Memorial Sloan Kettering Cancer Center, New York, New York. [4]Bioinformatics Institute (BII), Agency for Science, Technology and Research (A*STAR), Singapore. [5]Department of Medicine, Memorial Sloan Kettering Cancer Center, New York, New York. [6]Weill Cornell Medical College, New York, New York. [7]Center for Molecular Oncology, Memorial Sloan Kettering Cancer Center, New York, New York. [8]Antitumor Assessment Core Facility, Memorial Sloan Kettering Cancer Center, New York, New York. [9]Department of Oncology, University of Torino, Candiolo, Torino, Italy. [10]Candiolo Cancer Institute, FPO-IRCCS, Candiolo, Torino, Italy. [11]Department of Epidemiology and Biostatistics, Memorial Sloan Kettering Cancer Center, New York, New York. [12]The Shraga Segal Department of Microbiology, Immunology, and Genetics, Faculty of Health Sciences, Ben-Gurion University of the Negev, Beer-Sheva, Israel. [13]Department of Drug Discovery, Moffitt Cancer Center, Tampa, Florida. [14]Molecular Pharmacology Program, Memorial Sloan Kettering Cancer Center, New York, New York. [15]School of Biological Sciences, Nanyang Technological University, Singapore. [16]Department of Biological Sciences, National University of Singapore, Singapore.

Note: Supplementary data for this article are available at Cancer Discovery Online (http://cancerdiscovery.aacrjournals.org/).

J.E. Lee, S. Kannan, and A.M. Schram contributed equally to this article.

Corresponding Authors: Maurizio Scaltriti, Memorial Sloan Kettering Cancer Center, Room Z-1702, 1275 York Avenue, Box 20, New York, NY 10065. Phone: 646-888-3519; Fax: 646-422-0247; E-mail: scaltrim@mskcc.org; Emiliano Cocco, Memorial Sloan Kettering Cancer Center, Room Z-1702, 1275 York Avenue, Box 20, New York, NY 10065. Phone: 646-888-2721; E-mail: coccoe@mskcc.org; Chandra S. Verma, Bioinformatics Institute (A*STAR), 30 Biopolis Street, #07-01 Matrix, 138671 Singapore. Phone: 65-6478-8273; E-mail: chandra@bii.a-star.edu.sg; Andrea Ventura, Memorial Sloan Kettering Cancer Center, Zuckerman Research Laboratory, 417 East 68th Street, New York, NY 10065. Phone: 646-888-3068; Fax: 646-422-0871; E-mail: venturaa@mskcc.org; and Alexander Drilon, Memorial Sloan Kettering Cancer Center, 885 Second Avenue, New York, NY 10017. Phone: 646-608-3758; E-mail: drilona@mskcc.org

Cancer Discov 2021;11:126–41

doi: 10.1158/2159-8290.CD-20-0571

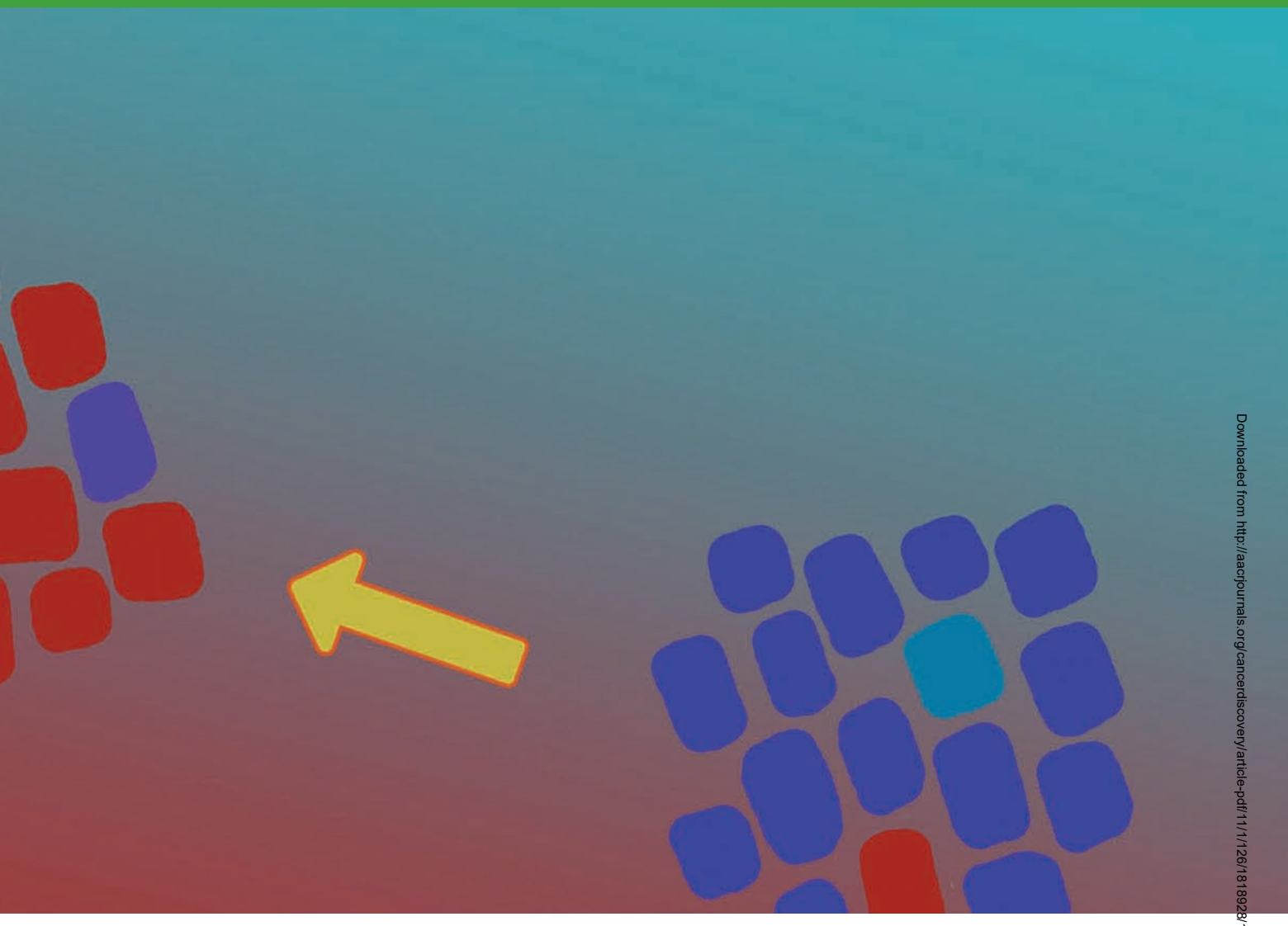

INTRODUCTION

Sequential tyrosine kinase inhibitor (TKI) therapy is an established strategy for cancers driven by an oncogenic kinase (1). Treatment is initiated with an early-generation TKI, and, upon the acquisition of resistance, a next-generation TKI is employed. This paradigm is typified by fusion-positive cancers for which rationally designed next-generation TKIs (lorlatinib for ALK fusions; repotrectinib for ROS1 fusions) have been shown to reestablish disease control in the face of kinase domain mutation–mediated resistance to earlier-generation inhibitors (crizotinib, ceritinib, or alectinib for ALK fusions; crizotinib or entrectinib for ROS1 fusions; refs. 2–4). The design of these next-generation agents is informed by a wealth of information on mechanisms that drive resistance to early-generation therapy (5).

Unfortunately, the dynamics that drive resistance to next-generation TKI therapy are more poorly characterized. In particular, although the evolutionary pressures of sequential TKI therapy propel the emergence of off-target/bypass track–mediated resistance in select cancers (4, 6), other cancers clearly acquire on-target resistance. On-target resistance mechanisms must induce structural changes in the kinase domain that ultimately impair the inhibitory effects of drug binding but simultaneously maintain kinase activity. Identifying and characterizing these mechanisms is an unmet need.

TRK fusion–positive cancers provide a prototype for the study of persistent on-target resistance in the context of sequential TKI therapy across lineage climates (7). First-generation TRK inhibitors such as larotrectinib and entrectinib are approved by multiple regulatory agencies for the treatment of TRK fusion–positive adult and pediatric cancers in a tumor-agnostic fashion (8–10). In response to first-generation therapy, many cancers will acquire kinase domain mutations that mediate resistance (8, 11, 12). Interestingly, these mutations result in amino acid substitutions in conserved regions that are paralogous to kinase domain substitutions that mediate resistance in other fusion-positive cancers. For example, the solvent-front substitutions TRKA^{G595R} and TRKC^{G623R} are paralogous to ALK^{G1202R} and ROS1^{G2032R} (4). The second-generation TRK inhibitors selitrectinib (LOXO-195, a selective TRK inhibitor)

and repotrectinib (TPX-0005, a multikinase TRK and ROS1 inhibitor) were designed to target many of these kinase domain mutations (13, 14). Both drugs are in prospective trials and have shown clinical activity in TRK fusion–positive cancers with kinase domain mutation–mediated resistance to the first-generation agents larotrectinib or entrectinib.

In this article, we study how TRK xDFG mutations can mediate resistance to second-generation TRK inhibitors. The xDFG residue maps immediately N-terminal to the DFG motif, an evolutionarily conserved triad across most kinases whose orientation defines the conformational states adopted by kinases (15). In an active or DFG-in conformation, the aspartate (D) of this motif points toward the ATP binding site, where it coordinates two Mg^{2+} ions. In the inactive or DFG-out state, the aromatic ring of the phenylalanine (F) residue flips by approximately 180°, moving the aspartate away from the ATP pocket with the consequent inhibition of catalytic activity (15). Small-molecule kinase inhibitors that bind to the active conformation of kinases (i.e., first- and second-generation TRK inhibitors available in the clinic) are classified as type I inhibitors and are canonical ATP competitors. In addition to the ATP-binding pocket, type II inhibitors also occupy an adjacent allosteric site (commonly referred to as the "back pocket") across the DFG motif; this back pocket is fully accessible only when the kinases are in the inactive conformation (16, 17).

Our study indicates that, although TRK xDFG substitutions represent a shared liability for type I TRK inhibitors, these substitutions represent a potential biomarker of sensitivity for type II multikinase inhibitors, drugs that bind to and stabilize the inactive conformations of TRK kinases and prevent their transition into the active state (17, 18).

RESULTS

TRKA xDFG Mutations Emerge with Second-Generation TRK Inhibitor Resistance

NTRK1 xDFG mutations resulting in G667 substitutions emerged in tumor DNA from patients with TRK fusion–positive cancers that progressed on second-generation TRK inhibitor therapy (Fig. 1). Patient 1, with a *TPM3–NTRK1*-fused, $TRKA^{G595R}$-mutant sarcoma, was treated with selitrectinib with limited durability. After 4 months of therapy, tumor sequencing at progression (pre- and post-selitrectinib samples obtained from the same lung metastasis site) showed the acquisition of a $TRKA^{G667C}$ (29% allele frequency) mutation and loss of the $TRKA^{G595R}$ solvent-front mutation (Fig. 1A). Patient 2, with a *LMNA–NTRK1*-fused, $TRKA^{G595R}$-mutant breast cancer, experienced a mixed response with selitrectinib. Cell-free DNA (cfDNA) collected after 2 months on therapy (coinciding with rapid liver metastasis growth) similarly demonstrated $TRKA^{G667C}$ acquisition and $TRKA^{G595R}$ loss (Fig. 1B). For Patient 1, $TRKA^{G667C}$ was found in the pretreatment sample at 0.3% (2/544 reads). Although the same analysis was not possible for Patient 2, these results suggest that preexisting $TRKA^{G667C}$-containing clones may have been selected by selitrectinib treatment.

Patient 3, with a *LMNA–NTRK1*-fused, $TRKA^{G595R}$-mutant colorectal cancer, received selitrectinib and developed resistance after 11 months of treatment. Sequencing of the resistant tumor revealed a new $TRKA^{G667A}$ mutation and persistence of the $TRKA^{G595R}$ mutation (Fig. 1C). These mutations were clonal, had similar allele frequencies (33% and 27%, respectively), and were found on the same allele in *cis* by RNA sequencing (Supplementary Fig. S1A). In parallel, in a $TRKA^{G595R}$-mutant colorectal cancer cell line that became resistant to repotrectinib after continuous drug exposure, we found that a new $TRKA^{G667C}$ substitution was acquired, whereas $TRKA^{G595R}$ was retained (Fig. 1D). The allele frequencies of these mutations were similar (63% and 65%, respectively), and RNA sequencing confirmed their occurrence in *cis* (Supplementary Fig. S1B). Proliferation assays and Western blot experiments conducted on this cell line showed that second-generation drugs failed to inhibit cell growth and TRK-activated downstream signaling, confirming its resistant phenotype (Fig. 1E and F).

Given that $TRKA^{G667}$ mutations were identified at the time of progression on second-generation TRK inhibitor therapy, we sought to evaluate whether these substitutions also confer primary resistance to the same agents. We identified two patients (Patients 4 and 5) who progressed on larotrectinib by acquiring $TRKA^{G667}$ mutations. Patient 4, with a *TPR–NTRK1*-positive non–small cell lung cancer, had a partial response (PR) on larotrectinib. Sequencing of cfDNA at progression identified the emergence of $TRKA^{G667S}$. Unfortunately, intrinsic resistance to selitrectinib was observed (patient received only 2 months of therapy; Supplementary Fig. S2A). Patient 5, with a *TPM3–NTRK1*-positive thyroid cancer, initially responded to larotrectinib, and sequencing of the cfDNA at progression identified multiple emergent TRKA kinase mutations, including $TRKA^{G667C}$ and $TRKA^{G667S}$. Similar to Patient 4, Patient 5 did not respond to selitrectinib (Supplementary Fig. S2B). Together, these clinical and preclinical findings suggest that TRKA xDFG substitutions (as single or compound mutations) limit sensitivity to second-generation TRK inhibitors.

TRKA xDFG Substitutions Compromise Second-Generation TRK Inhibitor Binding

To investigate the mechanism by which $TRKA^{G667}$ substitutions confer resistance to second-generation TRK inhibitors, we performed *in silico* molecular modeling combined with molecular dynamics (MD) simulations. Both second-generation TRK inhibitors currently in clinical testing, selitrectinib and repotrectinib, bind to the ATP-binding pocket of TRKA with an orientation that places their rigid fluoropyrimidine-containing aromatic moieties in close proximity to the glycine 667 residue. As such, substitution of the small glycine residue with any other amino acid, even those that have side chains with minimal additional bulk (e.g., the methyl side chain for alanine or the thiol side chain for cysteine), results in steric hindrance and compromises selitrectinib and repotrectinib binding (Fig. 2A). Consistently, binding free-energy calculations indicate that both selitrectinib and repotrectinib lose affinity for TRKA xDFG mutants when compared with wild-type (WT) TRKA (Supplementary Fig. S3A).

To confirm that $TRKA^{G667}$ mutations result in reduced activity of second-generation TRK inhibitors, we performed *in vitro* kinase assays using TRKA WT, $TRKA^{G595R}$ solvent-front mutant, and $TRKA^{G667}$ mutant kinases in the presence of increasing concentrations of selitrectinib or repotrectinib. Assays

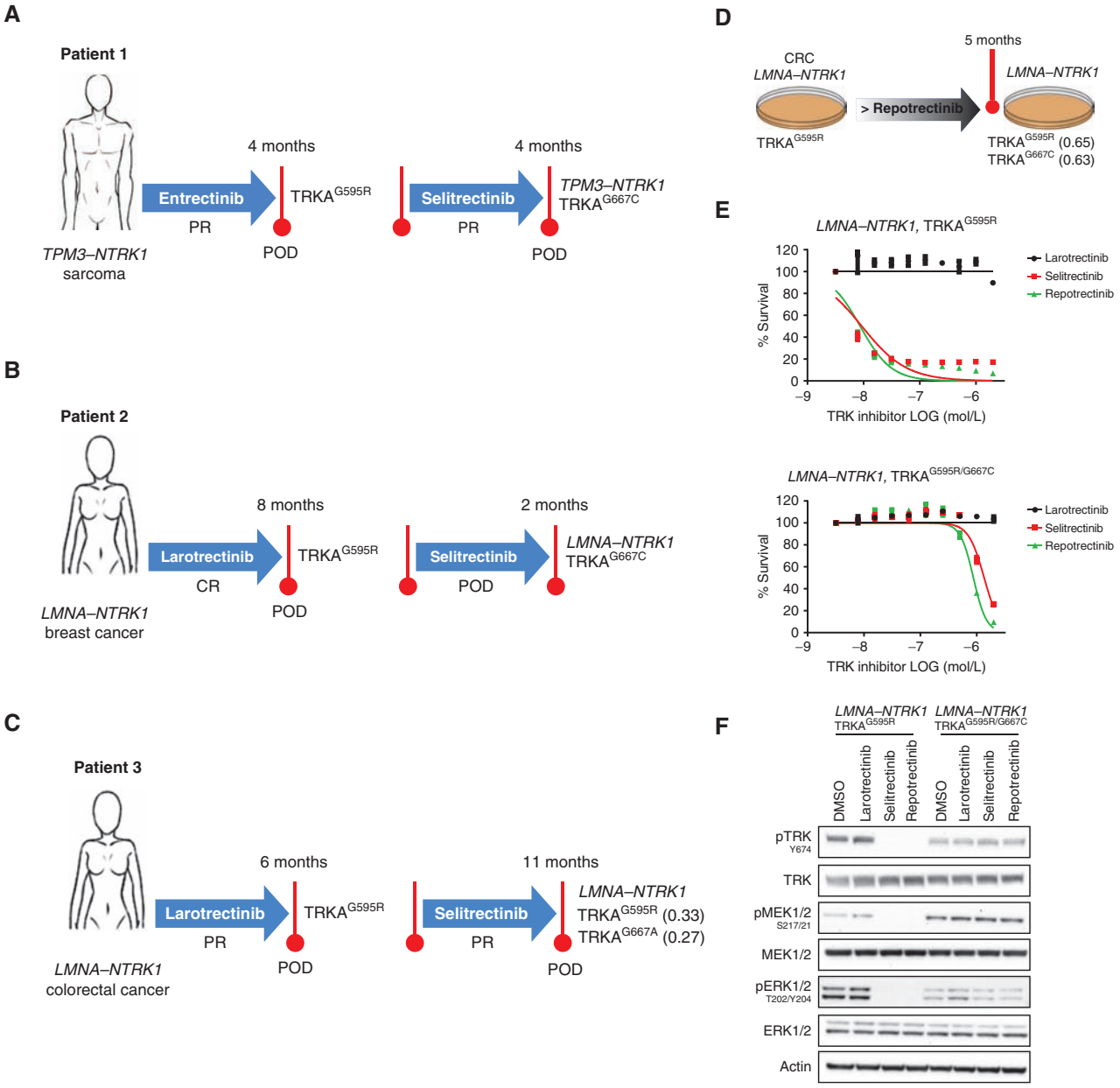

Figure 1. TRKA^{G667} mutations mediate resistance to second-generation TRK inhibitors in patients and preclinical models. **A–C,** The emergence of TRKA^{G667} mutations at progression on the second-generation TRK inhibitor selitrectinib in a patient with *TPM3–NTRK1*, TRKA^{G595R}-mutated sarcoma (Patient 1; **A**), a patient with *LMNA–NTRK1*, TRKA^{G595R}-mutated breast cancer (Patient 2; **B**), and a patient with *LMNA–NTRK1*, TRKA^{G595R}-mutated colorectal cancer (Patient 3; **C**). Although in both Patient 1 and Patient 2 the TRKA^{G595R} was not detected in the selitrectinib-resistant sample, this mutation persisted in the selitrectinib-resistant tumor of Patient 3 (the allele frequencies of the TRKA^{G595R} and the TRKA^{G667A} mutations are indicated in parentheses). All three patients were treated with a first-generation TRK inhibitor (entrectinib for Patient 1 and larotrectinib for Patients 2 and 3) prior to receiving selitrectinib and achieved partial responses (PR) or complete responses (CR). At progression, sequencing of the resistant tumors revealed the presence of a TRKA^{G595R} mutation in all three cases. **D,** The emergence of a TRKA^{G667C} mutation in a *LMNA–NTRK1*, TRKA^{G595R} mutated primary colorectal cancer (CRC) cell line that became resistant to the second-generation TRK inhibitor repotrectinb following chronic drug exposure. **E** and **F,** CellTiter-Glo–based proliferation assays (**E**) and Western blot analyses (**F**) confirming that the *LMNA–NTRK1*, TRKA$^{G595R/G667C}$ double-mutant colorectal cancer cell line is resistant to both selitrectinib and repotrectinib. POD, progression of disease.

conducted on single (TRKA^{G667C}) and double (TRKA$^{G595R/G667A}$ and TRKA$^{G595R/G667C}$) xDFG mutants showed that the calculated IC_{50} for selitrectinib was 429.7- to 8,514.3-fold higher compared with the IC_{50} obtained against TRKA WT and 12.3- to 238.4-fold higher compared with the IC_{50} obtained against the selitrectinib-sensitive TRKA^{G595R} solvent-front mutant (Fig. 2B). Similarly, the calculated IC_{50} values for repotrectinib against TRKA xDFG mutants were 59.1- to 1,863.6-fold higher compared with the IC_{50} obtained with TRKA WT and 2.1- to 66.1-fold higher than the IC_{50} calculated for the repotrectinib-sensitive TRKA^{G595R} solvent-front mutant (Fig. 2B). Together, these data indicate that TRKA xDFG

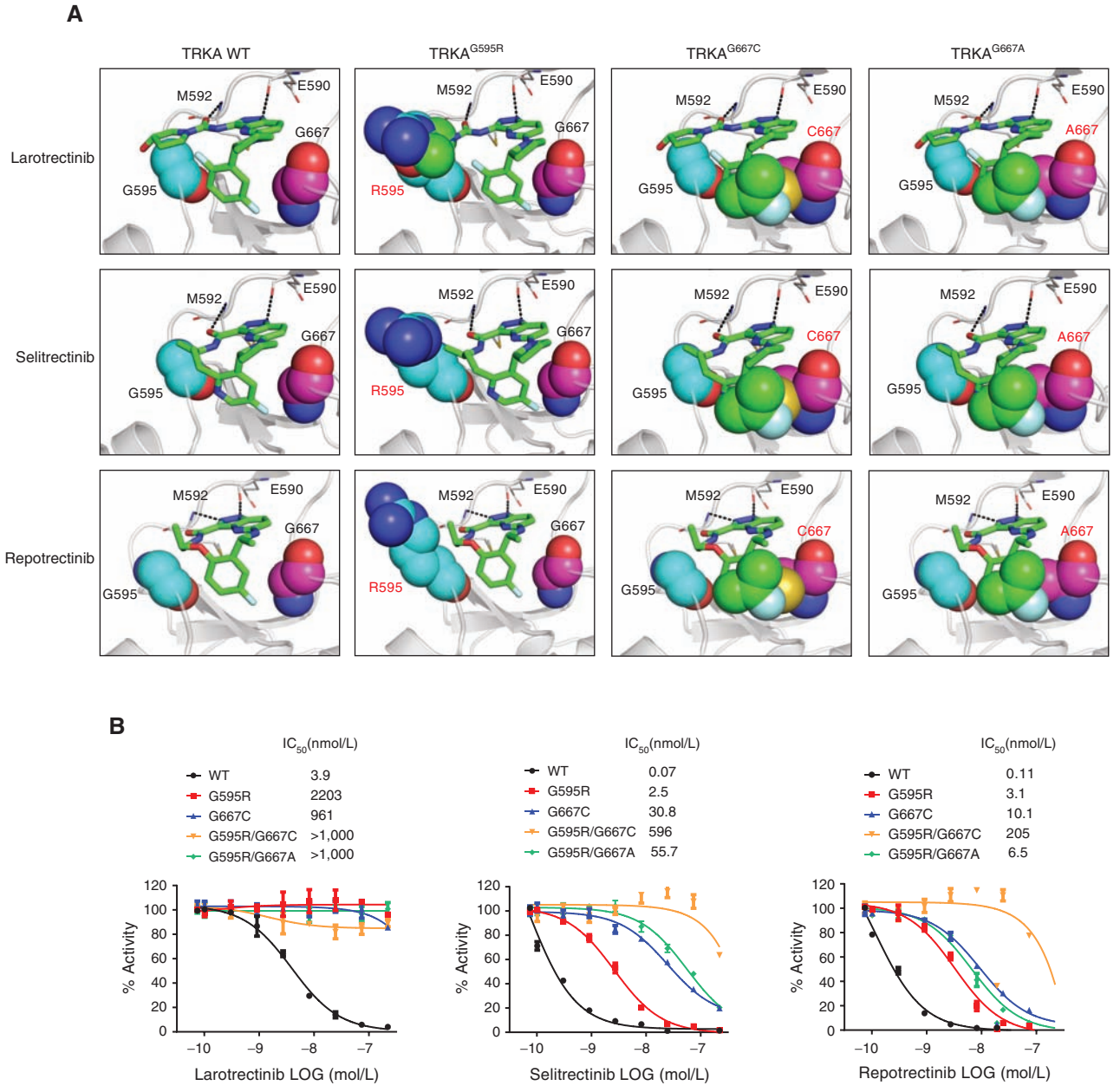

Figure 2. TRKA^{G667} substitutions generate steric hindrance that compromises selitrectinib and repotrectinib binding. **A,** Representative models from MD simulations showing larotrectinib, selitrectinib, and repotrectinib in complex with TRKA WT, TRKA^{G595R}, TRKA^{G667C}, and TRKA^{G667A} mutants. Bound drugs (green sticks) and kinase residues 595 and 667 (colored spheres) are displayed. Chemical groups of larotrectinib, selitrectinib, and repotrectinib that clash with mutant TRKA kinases are depicted as spheres for visualization purposes. **B,** Radiometric *in vitro* kinase assays showing the kinase activity of TRKA WT, TRKA^{G595R}, and TRKA^{G667C} single mutants and TRKA$^{G595R/G667C}$ and TRKA$^{G595R/G667A}$ double mutants treated with increasing concentrations of larotrectinib, selitrectinib, or repotrectinib. Kinase activities are presented as percent (mean ± SD) considering activity of 100% in the untreated kinases set as controls. IC_{50} values were calculated for each drug against the different kinases. Drug concentrations are represented as base 10 logarithm (LOG) on the x axis. Experiments were run in duplicate.

mutations limit sensitivity to selitrectinib and repotrectinib through impaired drug binding.

Type II TRK Inhibitors Preferentially Bind to and Inhibit TRKA, TRKC, and ROS1 xDFG Mutants

Existing data suggest that multikinase type II inhibitors can bind TRKA carrying the G667C substitution (19, 20). Therefore, we modeled TRKA xDFG and solvent-front mutants in complex with three type II inhibitors: cabozantinib, foretinib, and ponatinib (21, 22). Molecular dynamics simulations and binding free-energy calculations suggest that type II drugs can potentially bind the solvent-front, as well as all of the xDFG single- and double-mutant proteins, as the resultant substitutions are not predicted to generate steric hindrance (Fig. 3A; Supplementary Fig. S3B). Surprisingly, however, *in vitro* kinase assays showed that IC_{50} values calculated for

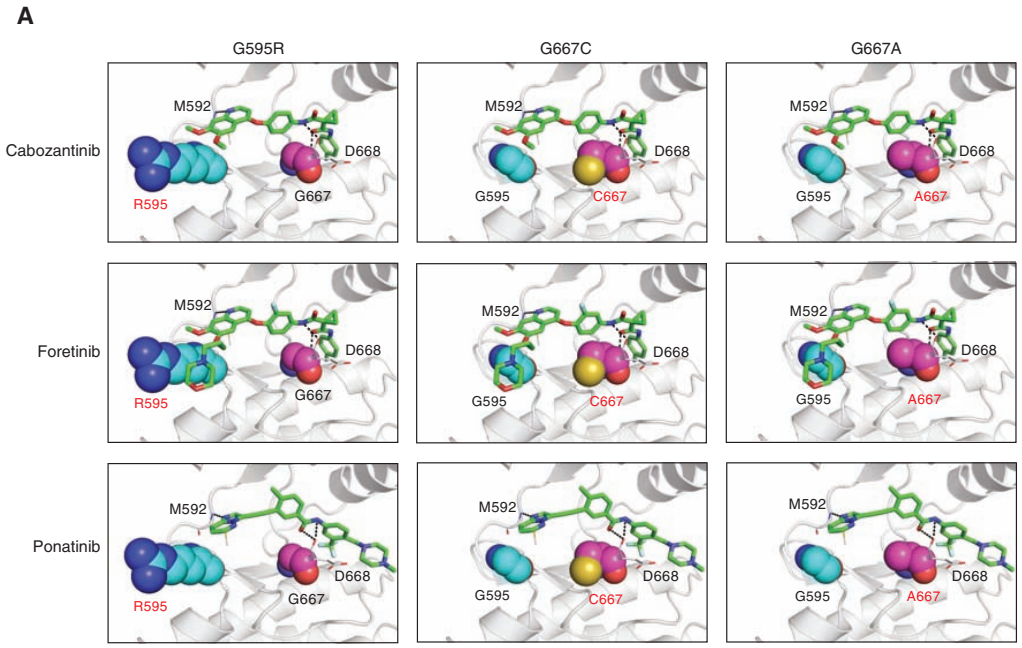

Figure 3. Type II TRK inhibitors preferentially bind to and inhibit the activity of TRKA xDFG mutants. **A,** Representative models of the most sampled conformations based on clustering the conformations generated during the MD simulations showing cabozantinib, foretinib, and ponatinib in complex with TRKA^{G595R}, TRKA^{G667C}, and TRKA^{G667A} mutants; clustering was carried out using the K-clust algorithm based on the root-mean-square deviation (RMSD) of the protein structures, and only one major cluster (representing >90% of the conformations sampled) was seen for each complex. Bound drugs (green sticks) and kinase residues 595 and 667 (colored spheres) are displayed. (*continued on next page*)

cabozantinib, foretinib, and ponatinib for TRKA xDFG single and double mutants were 3.4- to 579.3-fold lower than the IC_{50} for the solvent-front mutant and up to 72.3-fold lower than the IC_{50} for TRKA WT (Fig. 3B–3D), indicating that the presence of a TRKA xDFG substitution is sufficient to sensitize TRKA kinases to type II inhibitors. Interestingly, mutants with the Gly to Cys substitution in the xDFG codon of the TRKA kinases were found to be more sensitive to type II inhibitors than the double mutant harboring the Gly to Ala substitution, suggesting allele-specific sensitivity. Together, these results indicate that type II multikinase inhibitors may have higher affinity than type I second-generation TRK-specific inhibitors for TRKA xDFG mutants.

To test this hypothesis, we performed *in vitro* microscale thermophoresis to directly measure the binding affinity of cabozantinib/foretinib versus selitrectinib for the TRKA^{G667C}-mutant kinase. Our results show that the dissociation constants (Kd) for cabozantinib and foretinib were 8.84- and 10.74-fold lower than the Kd determined for selitrectinib, respectively (Fig. 3E). This suggests that TRKA xDFG substitutions may induce preferential adoption of the DFG-out conformation and increase type II inhibitor binding affinity, similar to data previously reported for the ERK2 kinase modified to harbor xDFG substitutions in mutagenesis-based assays (23). We then carried out all-atom MD simulations of apo-TRKA in its WT and mutant states. This analysis showed that, in the inactive conformation of the TRKA WT kinase, the xDFG residue (Gly667) is predicted to interact with the side chain of His648 of the His–Arg–Asp (HRD) motif that precedes the activation loop. Due to the flexibility of the Gly667 residue, this interaction is predicted to be weak, facilitating the transition of the TRKA WT kinase from the inactive to the active conformation (Fig. 3F, upper panel). When Gly667 is substituted with a Cys, the presence of the bulky side-chain group at this position is predicted to bring the carbonyl backbone of Cys667 and the side chain of the His648 into close proximity, thus stabilizing their interaction and favoring the inactive conformation. The distance between Gly667 and His648 in the TRKA WT in the inactive state is about 8 angstroms (Å) but reduces to approximately 3 Å when the Gly667 is substituted with the bulkier Cys (Fig. 3F, lower panel, and Supplementary Fig. S3C). According to this model, the reduced flexibility of the Cys667–His648 complex would increase the propensity of the mutated kinase to be stabilized in the inactive state (DFG-out), thus increasing the ability of cabozantinib and foretinib to bind the hydrophobic allosteric back pocket.

To study the generalizability of our findings, we next evaluated whether xDFG mutations also confer sensitivity to type II drugs in another member of the TRK kinases, TRKC, and in ROS1, a kinase that shares 39% identity with TRKA and can also form oncogenic fusions (24). *In vitro* radiometric assays showed that TRKC xDFG (G696A and G696C) and ROS1 xDFG (G2101A and G2101C) mutant recombinant kinases are exquisitely sensitive to type II inhibitors, drugs found to be less active against TRKC WT and ROS1 or TRKC and ROS1 solvent-front (G623R and G2032R, respectively) mutant kinases (Supplementary Fig. S4A and S4B).

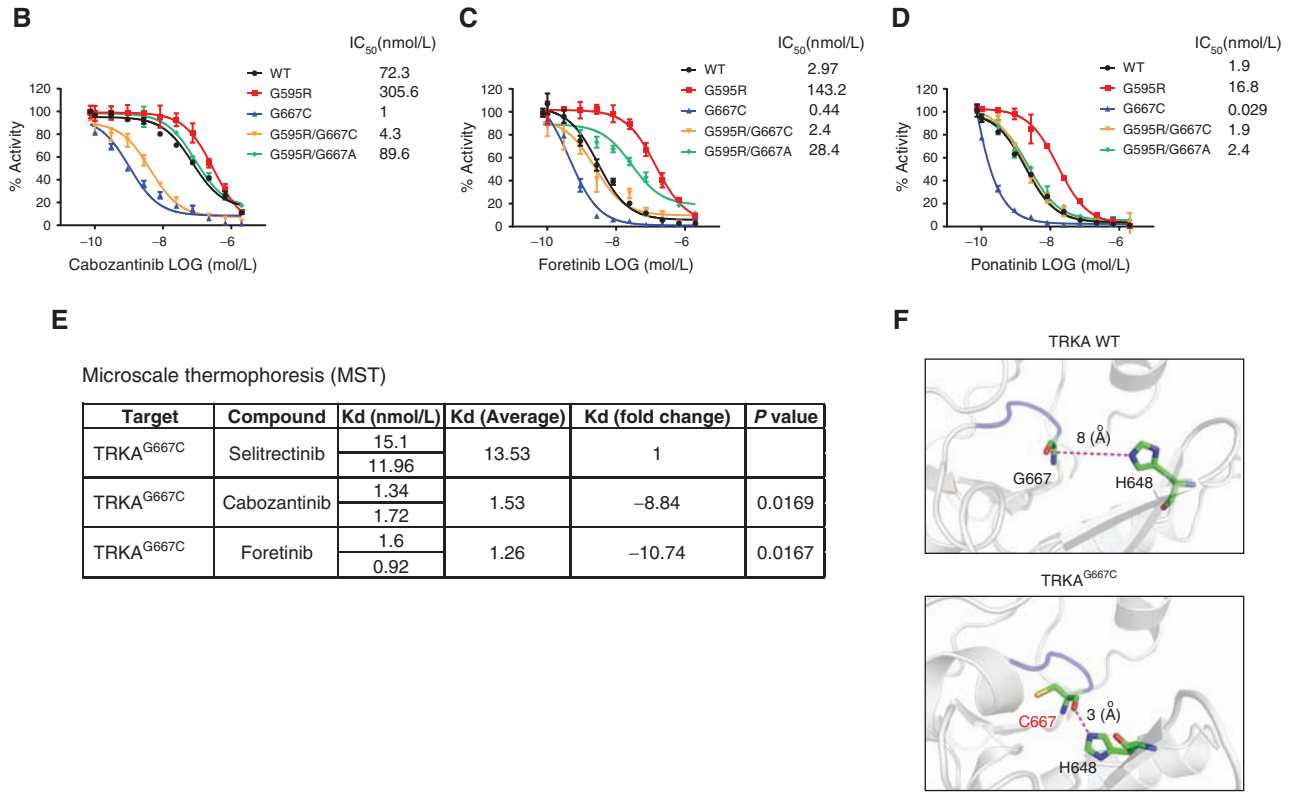

Target	Compound	Kd (nmol/L)	Kd (Average)	Kd (fold change)	*P* value
TRKA^{G667C}	Selitrectinib	15.1	13.53	1	
		11.96			
TRKA^{G667C}	Cabozantinib	1.34	1.53	–8.84	0.0169
		1.72			
TRKA^{G667C}	Foretinib	1.6	1.26	–10.74	0.0167
		0.92			

Figure 3. ***(Continued)*** **B–D**, Radiometric *in vitro* kinase assays showing the kinase activity of TRKA WT, TRKA^{G595R}, and TRKA^{G667C} single mutants and TRKA$^{G595R/G667C}$ and TRKA$^{G595R/G667A}$ double mutants treated with increasing concentrations of cabozantinib (**B**), foretinib (**C**), and ponatinib (**D**). Kinase activities are presented as percent (mean ± SD) considering activity of 100% in the untreated kinases set as controls. IC_{50} values were calculated for each drug against the different kinases. Drug concentrations are represented as base 10 logarithm (LOG) on the x axis. Experiments were run in duplicate. **E,** Determination of the binding affinity (Kd) of the type I inhibitor selitrectinib and type II inhibitors cabozantinib and foretinib for the TRKA^{G667C} mutant kinase in MST assays. Kd fold changes are indicated (average Kd of selitrectinib was set as reference). Experiments were run in duplicate, and *P* values were calculated using Student *t* test. **F,** Representative models of the most sampled conformations based on clustering the conformations generated during the MD simulations showing the interactions between the Gly667/Cys667 and His648 in the inactive forms of TRKA WT (top) and TRKA^{G667C} (bottom) kinases; clustering was carried out using the K-clust algorithm based on the RMSD of the protein structures, and only one major cluster (representing >90% of the conformations sampled) was seen for each complex. Kinases are shown in gray, the residues Gly/Cys667 and His648 are highlighted in green, and the interactions (hydrogen bonds) between residues are shown as magenta dashed lines.

Consistent with the biochemical assays, although cabozantinib slightly inhibited WT TRKC or ROS1 kinase phosphorylation when transfected in HEK293T cells, it markedly inhibited TRKC- or ROS1-mediated signaling when the same cells were transfected with the Gly to Cys xDFG TRKC or ROS1 mutants (Supplementary Fig. S4C and S4D). All atom MD simulations of apo-TRKC and ROS1 in their WT and mutant states also showed that the distance between the TRKC or ROS1 xDFG residue and the His677/1247 of the homology-directed repair (HDR) motifs reduced about threefold when the Gly 696/2101 were substituted with the bulkier Cys (Supplementary Fig. S4E and S4F). This is predicted to stabilize the mutated kinases in the DFG-out conformation, thus sensitizing to type II agents.

Because our data suggested that xDFG mutations induce structural changes that sensitize to type II drugs in multiple related kinases, we evaluated the prevalence of these mutations in the MSK-IMPACT cohort in 13 kinases that share high sequence identity with TRKA/B/C. Our analysis shows that xDFG mutations are recurrently found in several kinases, including RET, ALK, ROS1, EGFR, and ERBB2, in tumors of various histology, thus broadening the potential clinical relevance of our findings (Supplementary Fig. S4G).

xDFG Mutant *Bcan–Ntrk1*-Containing Mouse Gliomas Respond to Type II TRK Inhibitors

To test whether type II TRK inhibitors are effective against TRKA xDFG mutants in cell models, we used CRISPR/Cas9 to knock-in TRKA solvent-front and xDFG single and double mutations in tumor cells derived from a *Bcan–Ntrk1*-driven mouse model of glioma (Supplementary Fig. S5; ref. 25). Single- and double-mutant clones bearing the TRKA^{G598R} solvent-front mutation, the mouse ortholog to human TRKA^{G595R}, and/or the TRKA$^{G670C/A}$ xDFG substitutions, orthologs to human TRKA$^{G667C/A}$ (Fig. 4A–D and Supplementary Figs. S6A–S6J), were tested for their sensitivity to type I and type II TRK inhibitors. Consistent with our *in vitro* radiometric assays, *Bcan–Ntrk1*, TRKA xDFG single and double (xDFG and solvent-front) mutant cells were resistant to selitrectinib and repotrectinib but were sensitive to cabozantinib, foretinib, and ponatinib (Fig. 4E). Furthermore, type II drugs efficiently inhibited TRKA-mediated downstream

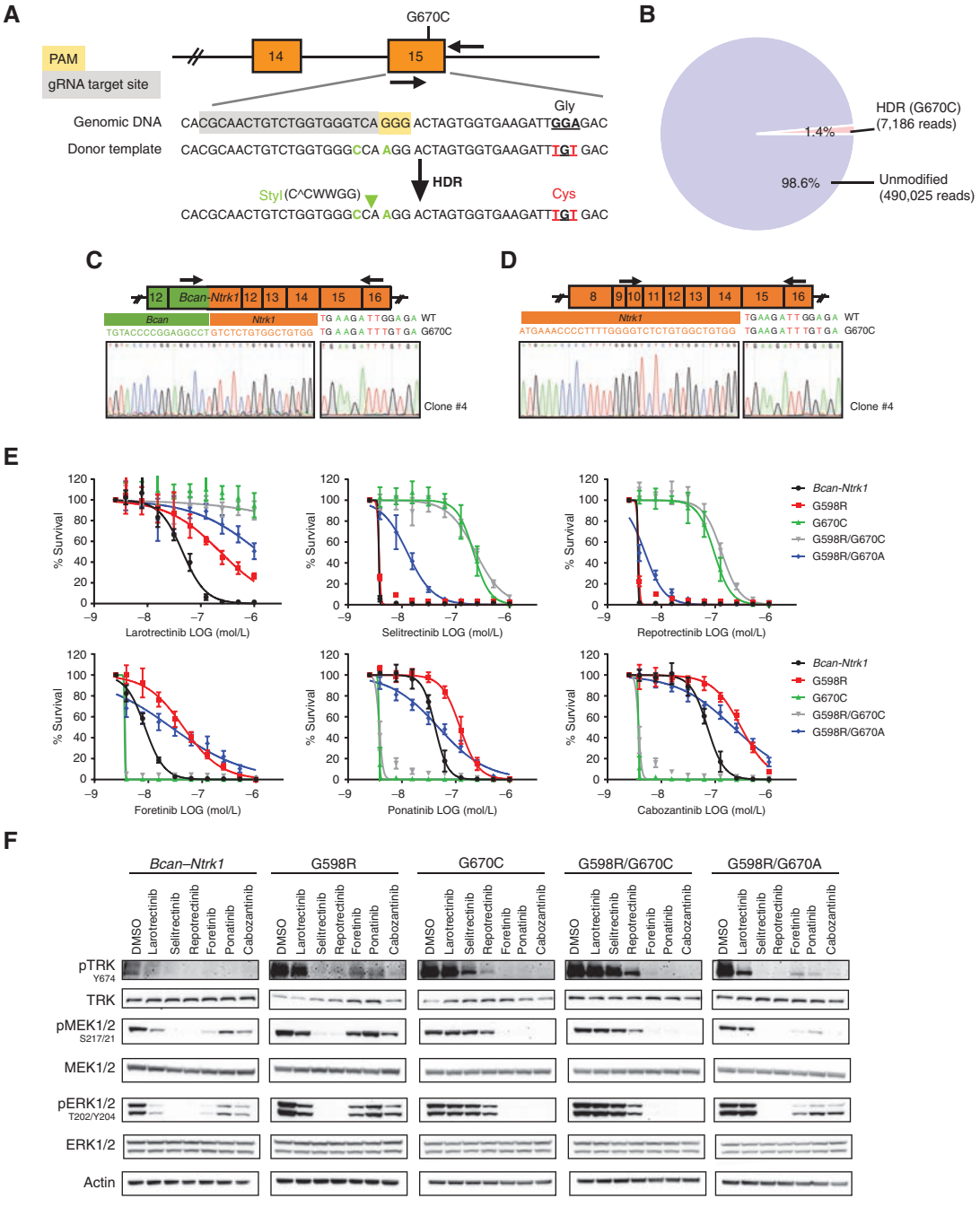

Figure 4. TRKA^{xDFG} mutated *Bcan–Ntrk1* mouse glioma cells respond to type II TRK inhibitors. **A–D,** Strategy for the generation of knock-in isogenic *Bcan–Ntrk1* glioma cells harboring the TRKA^{G670C} mutation. Sequences of genomic DNA (gRNA) and single-strand donor template are shown (**A**). Cys670 (TGT) substitution is indicated in red. Silent mutations (green) in the point accepted mutation (PAM, in yellow) and gRNA seed sequence creating a new restriction site (green arrow head) to facilitate clone selection are also shown. CRISPR/Cas9-induced HDR event counts for G670C mutation in a pooled cell population were determined after FACS by CRISPR sequencing (**B**). RT-PCR using primers (black arrows) designed to detect the *Bcan–Ntrk1* fusion transcript (**C**) or nonfused WT *NTRK1* transcript (**D**) was performed on total RNA. Sanger sequencing results of RT-PCR products are shown. **E** and **F,** CellTiter-Glo–based assays (**E**) and Western blot analyses (representative experiment of a total of three independent replicates; **F**) performed on the *Bcan–Ntrk1* WT and mutant clones showing the effect of type I (i.e., larotrectinib, selitrectinib, and repotrectinib) and type II (i.e., cabozantinib, foretinib, and ponatinib) TRK inhibitors on cell proliferation and TRKA-mediated downstream signaling. Proliferation assays are plotted as percent survival normalized on control, untreated cells. Data of three independent experiments are plotted as mean ± SD (**E**). (*continued on next page*)

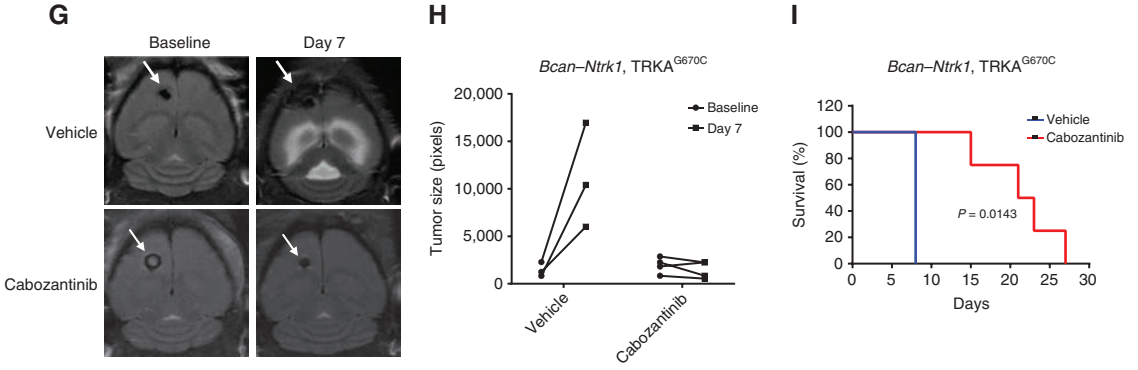

Figure 4. ***(Continued)*** **G,** Representative MRI scans of orthotopic mouse gliomas at baseline or 7 days after daily treatment with vehicle (top) or cabozantinib (100 mg/kg; bottom). **H,** Quantification of tumor size in vehicle-treated control mice ($n = 3$) and in cabozantinib-treated mice ($n = 4$) at baseline and after 7 days of daily treatment. Volume was calculated using ImageJ (in pixels). Each mouse was independently plotted. **I,** Survival curves of vehicle and cabozantinib-treated mice. Mice received daily treatment until sacrifice. Mantel–Cox test was used to calculate significant differences between the two groups. $P < 0.05$ was considered statistically significant.

signaling of TRKA single and double xDFG mutant clones (Fig. 4F). Similar results were obtained with two independent clones for each mutant (Supplementary Fig. S7A and S7B).

Resistance to selitrectinib and repotrectinib was reduced in xDFG mutants harboring the Gly to Ala substitution (TRKA double-mutant clones). These clones also displayed an intermediate sensitivity to cabozantinib, foretinib, and ponatinib, thus paralleling the kinase assay data obtained with this mutant. To further characterize the effect that the TRKA$^{G595R/G667A}$ double mutant has on drug response, we treated mouse glioma cells harboring this double mutation with increasing concentrations of selitrectinib or cabozantinib for 30 minutes or 24 hours and evaluated changes in the phosphorylation status of TRKA. Our results showed that, although both drugs were highly effective in inhibiting TRKA phosphorylation after 30 minutes of exposure, only cabozantinib maintained efficacy after 24 hours (Supplementary Fig. S7C). These data indicate that cabozantinib results in more durable pathway inhibition when compared with selitrectinib in the TRKA$^{G598R/G670A}$ double mutant, suggesting that cabozantinib may be more effective than selitrectinib in a chronic regimen or an *in vivo* setting.

To obtain mechanistic insights that could explain why type II inhibitors have increased activity specifically for TRK xDFG mutants, we investigated the biochemical properties of TRKA xDFG-mutant glioma cells. Proliferation and colony formation assays showed no differences in growth rate or oncogenic potential between cells harboring only the *Bcan–Ntrk1* fusion and cells also bearing the TRKA^{G670C} mutation. Cells harboring the solvent-front G598R single mutation and cells with the double mutations TRKA$^{G598R/G670A}$ and TRKA$^{G598R/G670C}$ were instead significantly slower and significantly less oncogenic than cells harboring the fusion only or cells also bearing TRKA^{G670C} (Supplementary Fig. S7D and S7E). Together, these data indicate that the increased sensitivity that xDFG single- and double-mutant cells show for type II inhibitors when compared with cells harboring the fusion only or with the TRKA^{G598R} solvent-front mutation is not the result of differences in the proliferation rate or the oncogenic properties of these mutants.

We then tested the antitumor activity of type II drugs in *Bcan–Ntrk1*, TRKA xDFG mutant cells injected intracranially into immunocompromised mice. One week after injection, we randomized mice into two groups and performed brain MRI. One group ($n = 3$) was treated with vehicle, and the other group ($n = 4$) was treated with cabozantinib. We chose cabozantinib as a representative type II TRK inhibitor because of its ability to cross the blood–brain barrier (26). MRI scans after 7 days of treatment showed that, although the tumor size of vehicle-treated mice increased up to 10-fold (accompanied by cerebral edema), cabozantinib prevented tumor growth (Fig. 4G and H). Accordingly, mice in the cabozantinib group survived significantly longer than mice in the control group (median of 8 vs. 22 days, respectively; $P = 0.0143$; Fig. 4I).

Type II TRK Inhibitors Overcome xDFG-Mediated Resistance in Patient-Derived Models

We next tested the antitumor activity of type II inhibitors in patient-derived models that became resistant to second-generation TRK inhibitors by acquiring TRKA xDFG mutations. Cell proliferation assays showed that these agents are highly active in inhibiting cell growth of the *LMNA–NTRK1*, TRKA$^{G595R/G667C}$ repotrectinib-resistant cell line (described in Fig. 1D–F) obtained following chronic drug exposure, but they are significantly less effective against the *LMNA–NTRK1*, TRKA^{G595R} parental counterpart (Fig. 5A). In agreement with this phenotype, type II but not type I drugs fully inhibited TRKA downstream signaling in this cell model (Fig. 5B).

To confirm that the activity of the type II multikinase inhibitors against the double-mutant cell line is the result of the specific inhibition of TRKA and not other targets, we tested the effects of crizotinib (MET inhibitor) and axitinib (VEGFR inhibitor) on cell viability and signaling. Results showed that only type II TRK inhibitors can induce cell death and inhibit TRKA-mediated signaling in the *LMNA–NTRK1*, TRKA$^{G595R/G667C}$ cell line (Supplementary Fig. S8A and S8B). Similarly, xenografts derived from this cell line demonstrated that cabozantinib treatment was sufficient to inhibit tumor growth (Fig. 5C).

Finally, we tested the efficacy of this type II inhibitor in patient-derived xenografts (PDX) established from the selitrectinib-

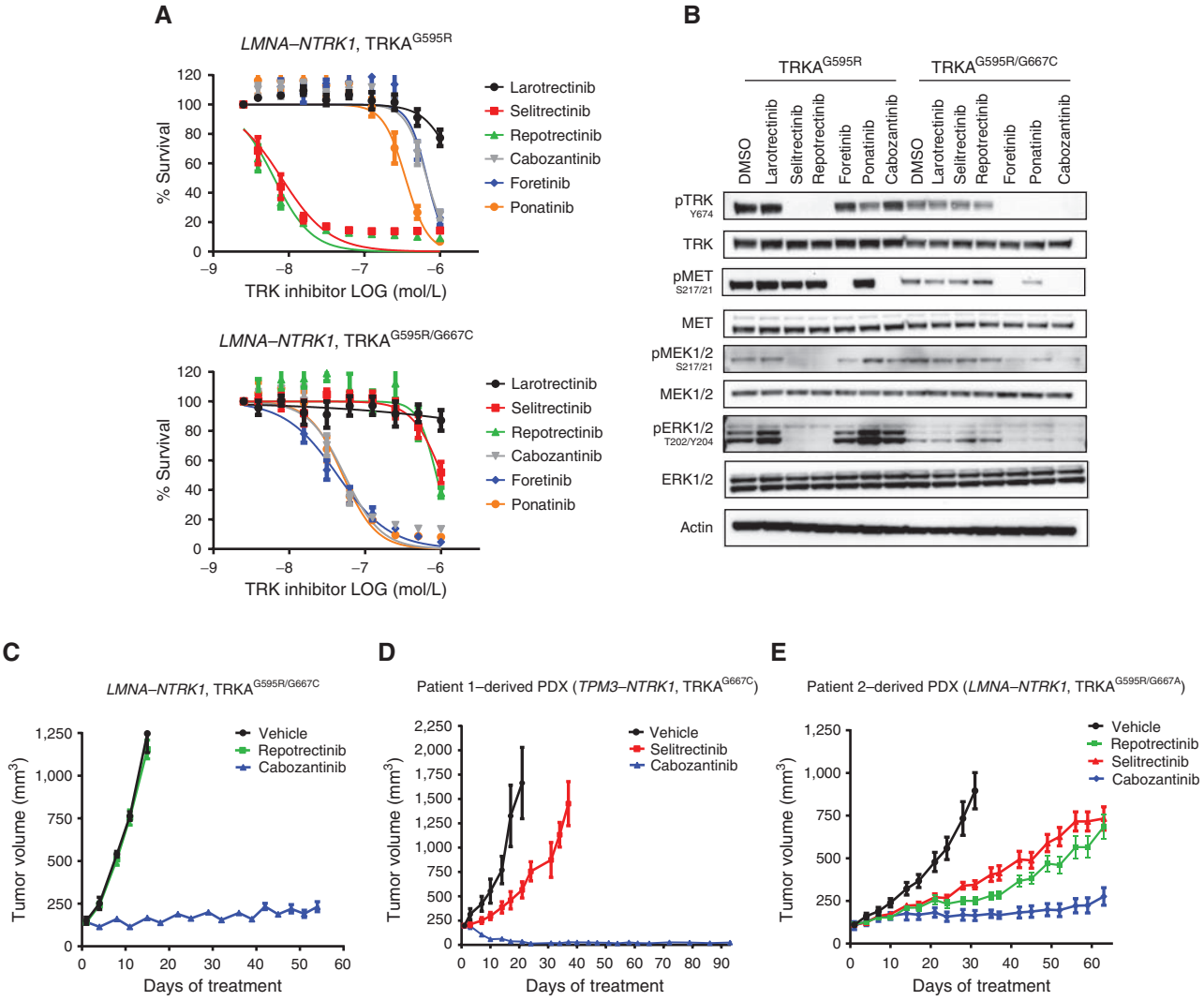

Figure 5. Type II drugs overcome resistance to second-generation TRK inhibitors in patient-derived models. **A** and **B,** CellTiter-Glo-based assays (**A**) and Western blot analyses (representative experiment of a total of three independent replicates; **B**) performed on the *LMNA–NTRK1*, TRKA^{G595R} and the *LMNA–NTRK1*, TRKA$^{G595R/G667C}$ double-mutant primary colorectal cancer cell lines showing the effect of type I (i.e., larotrectinib, selitrectinib, and repotrectinib) and type II (i.e., cabozantinib, foretinib, and ponatinib) TRK inhibitors on cell proliferation and TRKA-mediated downstream signaling. Proliferation assays are plotted as percent survival normalized on control, untreated cells. Data of three independent experiments are plotted as mean ± SD (**A**). **C–E,** *In vivo* efficacy of cabozantinib in xenografts established from the repotrectinib-resistant *LMNA–NTRK1*, TRKA$^{G595R/G667C}$ double-mutant primary colorectal cancer (**C**) and in PDXs established from the selitrectinib-resistant tumor of Patient 1 (*TPM3–NTRK1*, TRKA^{G667C} sarcoma; **D**) and Patient 3 (*LMNA–NTRK1*, TRKA$^{G595R/G667A}$ colorectal cancer; **E**).

resistant tumors of Patient 1 (*TPM3–NTRK1*, TRKA^{G667C} sarcoma) and Patient 3 (*LMNA–NTRK1*, TRKA$^{G595R/G667A}$ colorectal cancer). Tumors derived from Patient 1 treated with cabozantinib achieved a complete and durable (3 months) response (Fig. 5D), whereas durable (2 months) disease control was observed in tumors derived from Patient 3 (Fig. 5E). Taken together, these data indicate that type II TRK inhibitors can overcome acquired resistance to second-generation type I inhibitors mediated by the acquisition of xDFG mutations.

DISCUSSION

The emergence of on-target mutations that predispose oncogenic kinases to switch conformational states represents a largely underappreciated mechanism of targeted therapy resistance. Here, we demonstrate that xDFG mutations are recurrently identified in patients and preclinical models from diverse histologies of TRK fusion–positive cancers refractory to second-generation TRK inhibitor therapy. Clones with xDFG mutations can either be present *de novo* or be acquired with TKI therapy.

Structural modeling and biochemical studies reveal that xDFG substitutions not only limit TRK inhibitor binding by generating steric hindrance but also result in preferential adoption of the inactive DFG-out conformation by TRK kinases. Our experiments show that neither differences in growth rate nor the oncogenic potential of these xDFG mutants can explain DFG-out conformation adoption. We

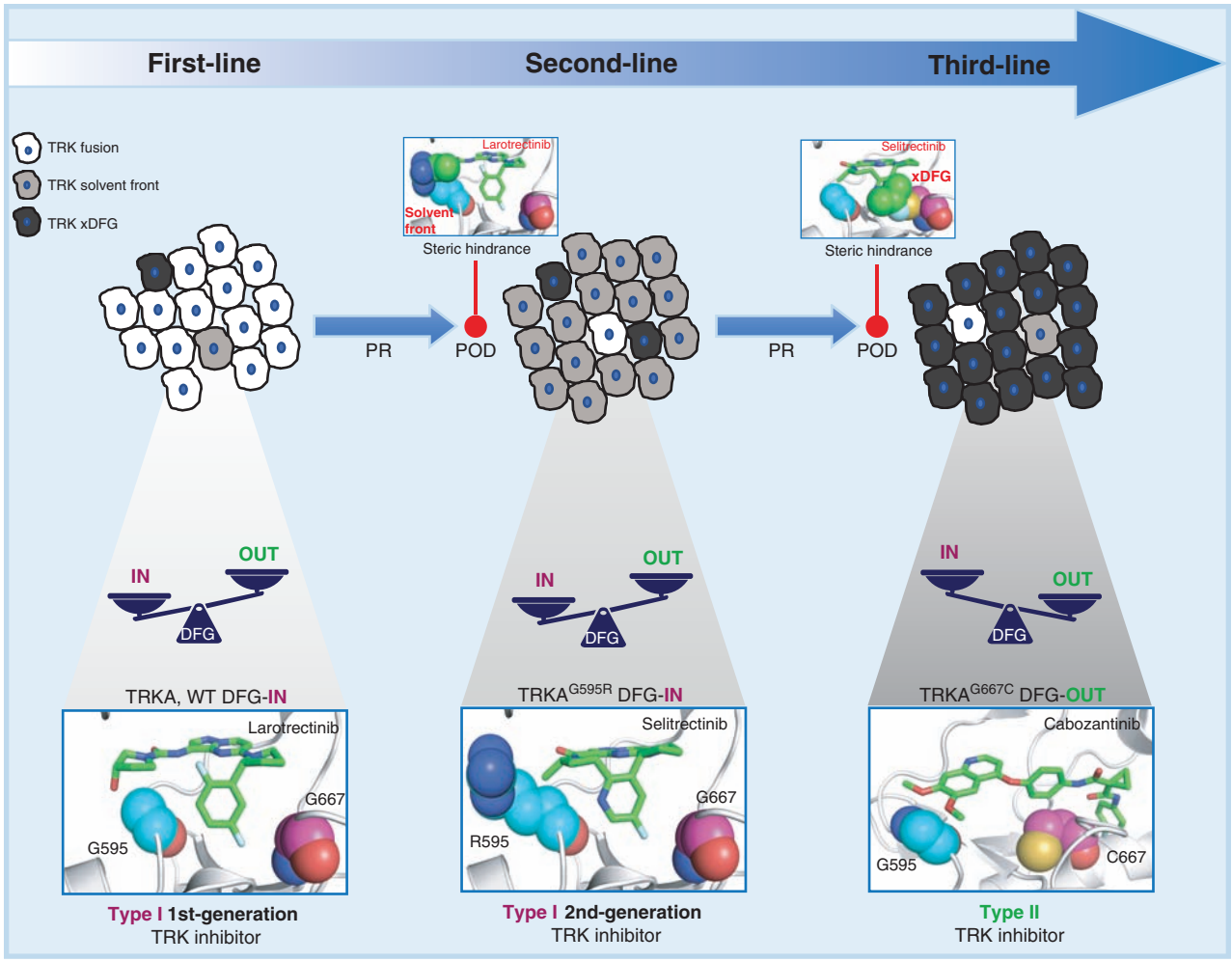

Figure 6. Proposed model of sequential therapy in *NTRK* fusion–positive tumors. At diagnosis, tumors are mainly composed of WT TRK fusion–positive cells. The pool of kinase molecules in the DFG-in conformation is prevalent, and patients are treated with type I, first-generation TRK inhibitors (first-line therapy: larotrectinib). At progression, the most prevalent mechanism of on-target resistance is the emergence of TRK solvent-front mutations that generate steric hindrance, thus compromising first-generation drug activity. In cells harboring TRK solvent-front mutations, the pool of DFG-in kinase molecules is still predominant, and patients are treated with type I second-generation TRK inhibitors (second-line therapy: selitrectinib). At progression, the emergence of TRK^{xDFG} single and double mutations generates steric hindrance, compromising the binding of type I second-generation TRK inhibitors, and induces the kinase to preferentially adopt its inactive DFG-out conformation, sensitizing to type II kinase inhibitors (proposed third-line therapy). Note that only on-target mechanisms of resistance are displayed in this model.

thus posit that xDFG substitutions induce structural changes that delay the transition of these kinase molecules from the DFG-out to the DFG-in conformation. This, in turn, could increase the sensitivity of these mutants for type II inhibitors, drugs that specifically engage the DFG-out kinase state (Fig. 6). This highlights that genomic interrogation alone across fusion-positive cancers may be insufficient to understand the complex steric and conformational changes that govern drug resistance and sensitivity.

It is important to recognize several factors. First, the crystal structures of type II inhibitors have yet to be complexed with TRK kinases to confirm type II binding. We likewise cannot rule out that these drugs bind to TRK via mechanisms beyond simple type II engagement. Second, not all xDFG substitutions are created equal; the size and charge of the substituted amino acid may induce differential phenotypes. For example, we found that TRKA^{G670C}-containing models harbored more resistance compared with TRKA^{G670A}-containing models. The larger size of the cysteine (compared with alanine) and the partial negative charge on its sulfur atom may result in more steric hindrance and repulsion of the negatively charged fluoro-containing aromatic groups of the second-generation TRK inhibitors selitrectinib and repotrectinib. It is thus possible that G→A xDFG substitution-containing cancers could respond initially to therapy, but with less durability compared with cancers harboring other on-target resistance mechanisms.

xDFG mutations were initially identified as acquired resistance mechanisms to first-generation type I TRK inhibitors (8, 12). Second-generation TKIs were thus designed to maintain activity against these and other more common resistance mutations. A primary design parameter of these small

macrocyclic agents was the ability to abrogate steric hindrance resulting from solvent-front and gatekeeper residue substitutions. Although second-generation TKIs were effective against many of these resistance mutations, these drugs were still designed as type I inhibitors. As such, these agents were not poised to avoid the penalties of structural shifts into the inactive conformation. Our work thus exposes an occult liability that was not predicted by initial experiments and highlights the inability of second-generation type I TKIs to overcome all forms of on-target resistance.

These observations are potentially applicable to other oncogenic kinases. We demonstrate, for example, that xDFG substitutions not only occur across other kinases known to be involved in recurrent gene fusions but also confer sensitivity to type II inhibitors in the context of *ROS1* fusions. It should be noted that adaptive conformational resistance engendered by altering the relative proportion of active or inactive kinase pools can occur in either direction. In BCR–ABL-containing chronic myelogenous leukemia, resistance mutations to first-generation TKI therapy with the type II TKI imatinib result in a preferential shift toward an active DFG-in conformation (27), the opposite of what is observed in TRK xDFG resistance. The emergence of mutations that induce conformational shifts has also been reported in EGFR-, MET-, KIT-, RET-, and ROS1-driven cancers (28–32).

We show that type II inhibitors overcome xDFG resistance by binding the preferred inactive conformation of these mutant kinases. Although several TKIs are known to engage kinases in an inactive conformation, the vast majority of these agents (e.g., cabozantinib/foretinib) are repurposed multikinase inhibitors that were not intentionally designed to inhibit select targets (33). Therefore, they are characterized by substantial off-target inhibition and consequently a high frequency of side effects and poor plasma exposures (34). In addition, these agents represent a minority of TKIs that are available in the clinic, as most targeted therapies that are either approved (i.e., osimertinib, alectinib, brigatinib, lorlatinib, and entrectinib) or in trials are type I inhibitors (35). Rational drug design should thus move toward the development of selective type II kinase inhibitors. Although this can be challenging, particularly considering the heterogeneity of mutations that might be amenable to type II kinase inhibition, methods to test the affinity of candidate TKIs against multiple mutation variants have already been reported (36).

In conclusion, our study has uncovered a molecular switch induced by xDFG mutations that limits the sensitivity to type I kinase inhibitors. This occurs via the generation of steric hindrance and the induction of conformational changes that favor the inactive DFG-out kinase state. This same switch, in turn, sensitizes these mutant kinases to type II inhibitors that effectively engage the inactive conformation. Ultimately, a combination of selective type I and type II inhibitors might represent the most effective way to address on-target mechanisms of TKI resistance.

METHODS

Patients

Patients were treated with TRK inhibitors as part of prospective Institutional Review Board (IRB)–approved research protocols or expanded-access protocols. All patients provided written informed consent for genomic sequencing of tumor DNA and cfDNA; for the review of medical records for detailed demographic, pathologic, and clinical data; and for publication of this information as part of an institutional IRB-approved research protocol [Memorial Sloan Kettering Cancer Center (MSKCC), NCT01775072]. Research protocols for tumor collection and analysis were approved by the ethical committees of the MSKCC.

Compounds

Larotrectinib and selitrectinib were obtained from Loxo Oncology. Repotrectinib was purchased from Selleckchem. Cabozantinib, foretinib, ponatinib, crizotinib, and axitinib were purchased from MedChem Express. All drugs were dissolved in DMSO to yield 10 mmol/L stocks and stored at −20°C.

Targeted Tumor Sequencing

DNA from formalin-fixed, paraffin-embedded tissue and matched germline DNA underwent targeted next-generation sequencing assay using MSK-IMPACT (37). In brief, this assay uses a hybridization-based exon capture designed to capture all protein-coding exons and select introns of oncogenes, tumor-suppressor genes, and key members of pathways that may be actionable by targeted therapies. In this study, either 410 or 468 key cancer-associated genes were analyzed. Sequencing data were analyzed as previously described to identify somatic single-nucleotide variants, small insertions and deletions, copy-number alterations, and structural rearrangements (38). In addition, hotspot alterations were identified using an adaptation of a previously described method (39) applied to a cohort of 24,592 sequenced human cancers (40).

Targeted Plasma Sequencing

Cell-free DNA was extracted from all plasma samples and sequenced using a custom, ultradeep coverage, next-generation sequencing panel (MSK-ACCESS). The custom assay includes key exons and domains of 129 and introns of 10 genes harboring recurrent breakpoints and uses duplex unique molecular identifiers (UMI) and dual-index barcodes to minimize background sequencing errors and sample-to-sample contamination. Sequencing data were analyzed using a custom bioinformatics pipeline that trims the UMIs, aligns the processed reads to the human genome, collapses PCR replicates into consensus sequences, and realigns the error-suppressed consensus reads. Consensus reads with representation from both strands of the original cfDNA duplex were used for *de novo* variant calling using VarDict (v1.5.1). Mutation calling required at least one collapsed read at a known cancer hotspot site or at least three collapsed reads at non-hotspot sites. All samples were sequenced to an average depth of approximately 20,000× coverage. Somatic mutations were identified and quantified as variant allele frequencies. Copy-number alterations were identified across all samples using a previously described method (38). *NTRK* fusions were identified and quantified using Manta (v1.5.0). All samples were manually reviewed to identify *NTRK* fusions. Variants were called against an unmatched healthy plasma donor to identify any specimen type–related artifacts. Mutations called at silent, intronic, and intergenic loci were removed.

Structure Preparation

The structures of the apo forms of TRKA in its inactive state and of TRKA in its active state were generated using the available crystal structures. A crystal structure of apo-TRKA in its inactive state (PDB: 4F0I) is available. The structure of the active form of apo-TRKA was generated from the crystal structure of TRKA complexed to a ligand (PDB: 4YNE) by removing the ligand. The three-dimensional structures of the drug molecules larotrectinib, selitrectinib, and

repotrectinib were built using Maestro and minimized using the Macromodel module employing the OPLS-2005 force field (41) in Schrödinger 9.0. All of the drug molecules were then prepared with Ligprep, which generates low-energy tautomers and enumerates realistic protonation states at physiologic pH. The prepared inhibitors were docked into the ATP-binding pocket of the apo forms of TRKA kinase generated above using Glide (42). The docking was carried out under a constraint that a hydrogen bond is formed between the nitrogen atoms from the drug molecules and the backbone amide nitrogen of Met592 in TRKA; this was imposed based on the observation of such a hydrogen bond in the crystal structures of the ROS1 kinase complexed to Ent (Ent is a drug very similar to the drugs considered here; PDB: 5KVT) and of TRKA in its active state complexed to a ligand (also very similar to the drugs that are being studied here; PDB: 4YNE). A box of size $10 \times 10 \times 10$ Å for molecular docking, centered on the ATP-binding site residues of TRKA in its active state, was used to define the search space of each docked drug molecule. For the grid generation, the default Glide settings were used. The docked conformation of each ligand was evaluated using the Glide Extra Precision (XP) scoring function. The structural models of the drug molecules foretinib and ponatinib complexed to the inactive states of TRKA were generated using the co-crystal structures of foretinib bound to the inactive state of MET kinase (~39% identity to TRKA; PDB: 6SD9) and of ponatinib bound to the inactive state of FGFR4 kinase (~41% identity to TRKA; PDB: 4TYI). Both of these complex structures were superimposed onto the structure of the inactive state of TRKA and the corresponding complexes of TRKA with foretinib and ponatinib generated. The structural model of cabozantinib complexed to the inactive state of TRKA was generated by modifying foretinib in its complexes with TRKA.

Structural models of the apo forms and complexes of the mutant kinases in both active and inactive forms (G595R, G667C, G667A, G667S, G595R/G667C, and G595R/G667A) with the six drug molecules (larotrectinib, selitrectinib, repotrectinib, cabozantinib, foretinib, and ponatinib) were modeled using the corresponding structures of the WT kinases using the prime module (the side-chain orientations of the mutations are optimized) from the Schrödinger software. All of the structural models were subsequently subjected to MD simulations for further refinement.

Molecular Dynamics Simulations

MD simulations were carried out with the pmemd.cuda module of the program Amber18 (43). The partial charges and force field parameters for each drug molecule were generated using the Antechamber module in Amber. All atom versions of the Amber14SB force field (ff14SB; ref. 44) and the general Amber force field (GAFF; ref. 45) were used to model the protein and the drug molecules, respectively. The Xleap module of Amber was used to prepare the systems for the MD simulations. All of the simulation systems were neutralized with appropriate numbers of counter ions. Each neutralized system was solvated in an octahedral box with TIP3P (46) water molecules, leaving at least 10 Å between the solute atoms and the borders of the box. All MD simulations were carried out in explicit solvent at 300 K. During the simulations, the long-range electrostatic interactions were treated with the particle mesh Ewald (47) method using a real-space cutoff distance of 9 Å. The Settle (48) algorithm was used to constrain bond vibrations involving hydrogen atoms, which allowed a time step of 2 fs during the simulations. Solvent molecules and counter ions were initially relaxed using energy minimization with restraints on the protein and drug atoms. This was followed by unrestrained energy minimization to remove any steric clashes. Subsequently, the system was gradually heated from 0 to 300 K using MD simulations with positional restraints (force constant: 50 kcal mol^{-1} $Å^{-2}$) on protein and drugs over a period of 0.25 ns, allowing water molecules and ions to move freely. During an additional 0.25 ns, the positional restraints were gradually reduced followed by a 2-ns unrestrained MD simulation to equilibrate all the atoms. Finally, production MD simulations were carried out for 250 ns in triplicate, with conformations stored for every 10 ps. Simulation trajectories were visualized using VMD (49), and figures were generated using PyMOL (50). A summary of production of MD simulation details and time of simulations is reported in Supplementary Tables S1A–C.

In Vitro *Kinase Assays*

Recombinant kinases were purchased by SignalChem Lifesciences Corporation. *In vitro* kinase assays were performed by Reaction Biology Corp. Briefly, compounds (larotrectinib, selitrectinib, cabozantinib, foretinib, and ponatinib) were tested in 10-dose IC_{50} mode with threefold serial dilution starting at 2 μmol/L in the presence of 10 μmol/L ATP. Control compound Staurosporine was also tested. Two replicates for each dilution were performed. IC_{50} was calculated using GraphPad Prism 8.

Microscale Thermophoresis

Microscale thermophoresis (MST) experiments were conducted by Reaction Biology Corp. Selitrectinib concentrations ranged from 0.015 to 1000 nmol/L (16 doses), and cabozantinib and foretinib concentrations ranged from 0.003 to 100 nmol/L (16 doses). The concentration of the target ($TRKA^{G667C}$) was kept constant at 5 nmol/L. Two independent experiments were performed for each drug. Student *t* test was used to calculate significant differences in Kd values. $P < 0.05$ was considered statistically significant.

Culture of Bcan–Ntrk1 *Mouse Glioma Cells*

All mouse $p53^{-/-}$ *Bcan–Ntrk1* glioma cell lines were plated on laminin-coated dishes and cultured in Neurocult Stem Cell Basal Media with Proliferation Supplements (Stem Cell Technologies). The low-density seeding method was performed to isolate a monoclonal cell line harboring desired mutation from an electroporated pooled population of mouse $p53^{-/-}$ *Bcan–Ntrk1* glioma cells.

CRISPR/Cas9-Mediated Homology-Directed Repair

The Cas9–gRNA ribonucleoprotein (RNP) complex and single-stranded oligodeoxynucleotides (ssODN) were used to generate TRKA mutations in *Bcan–Ntrk1* mouse glioma cells. We used a CRISPR/Cas9-mediated HDR approach in which cells were nucleofected with the Cas9–gRNA ribonucleoprotein complex together with single-stranded oligodeoxynucleotides (donor template sequences) that harbored the desired substitutions plus additional silent substitutions designed to introduce a diagnostic restriction site.

All CRISPR RNAs (crRNA; Alt-R CRISPR-Cas9 crRNA) and ssODNs are synthesized by Integrated DNA Technologies, and the RNP complex was formed according to the manufacturer's instructions. Sequences of crRNAs and ssODNs can be found in Supplementary Table S2A. Briefly, gRNA was assembled by mixing equimolar amounts of crRNA and trans-activating crRNA (tracrRNA; Alt-R CRISPR-Cas9 tracrRNA-ATTO-550) and heating to 95°C for 5 minutes. Cas9 (Alt-R S.p. Cas9 Nuclease V3) and gRNA were incubated for 10 minutes at room temperature to allow RNP formation. The ssODNs and RNP complex were delivered into 1×10^5 mouse $p53^{-/-}$ *Bcan–Ntrk1* glioma cells by the 4D-Amaxa Nucleofector System (Lonza) using the Amaxa SF Cell Line Nucleofector X Kit S (Lonza) according to the manufacturer's instructions. Cells were sorted based on ATTO-550 expression 48 hours post-nucleofection by the Flow Cytometry Core Facility at MSKCC.

PCR and Reverse Transcription PCR for Clone Selection

For PCR analysis of genomic DNA, cells were collected and genomic DNA was extracted by phenol:chloroform:isoamyl alcohol

(Invitrogen). For reverse transcription PCR, total RNA was isolated from cells using TRIzol reagent (Invitrogen), and cDNA was generated using the SuperScript III First-Strand Synthesis System (Invitrogen). The primers used in the various PCR reactions are provided in Supplementary Table S2B.

CRISPR Sequencing

An approximately 200-bp region encompassing the modified locus targeted by CRISPR was PCR-amplified from isolated genomic DNA, and the amplicon was gel-purified (New England BioLabs). Each amplicon was sequenced to 75,000 to 100,000 reads sequencing. Reads were analyzed using CRISPResso by the MSKCC Integrated Genomics Operation.

Drug Screenings

For the CellTiter-Glo Cell Viability Assay (Promega), *LMNA–NTRK1*, TRKA^{G595R} and *LMNA–NTRK1*, TRKA$^{G595R/G667C}$ primary colorectal cancer cell lines or the isogenic mouse glioma cell lines were seeded in 96-well plates (6,000 per well). The following day, larotrectinib, selitrectinib, repotrectinib, cabozantinib, foretinib, ponatinib, crizotinib, or axitinib (1:2 dilutions starting with a maximum concentration of 1000 nmol/L) was added. CellTiter-Glo reagent was added 72 hours later, and absorbance was read at 490 nm according to the manufacturer's protocol. Data are presented as percent cell viability (mean ± SD) normalized to the DMSO-treated cells considered 100% viable. Drug concentrations are represented as base 10 logarithm (LOG) on the x axis.

Antibodies and Western Blots

Cells were seeded in six-well plates (500,000) per condition in full medium. The day after, cells were treated with 50 nmol/L of each compound for 30 minutes. Total protein lysates were extracted using radioimmunoprecipitation assay buffer and quantified using bicinchoninic acid according to the manufacturer's protocol. Lysates were separated using sodium dodecyl sulfate–polyacrylamide gel electrophoresis gels according to standard methods. Membranes were probed using the following antibodies: pan TRK clone A7H6R (92991S, Cell Signaling Technology); phospho-TRKA (Y674/675) clone C50F3 (4621S, Cell Signaling Technology); phospho-MEK1/2 (S217/221) clone 41G9 (9154S, Cell Signaling Technology); total MEK1/2 (9122L, Cell Signaling Technology); phospho-p44/42 MAPK (Erk1/2; T202/Y204) clone D13.14.4E (4370S, Cell Signaling Technology); total ERK1/2 (9102S, Cell Signaling Technology); phospho-Met (Tyr1234/1235) (3129S, clone 3D7, Cell Signaling Technology); total Met (8198S, clone D1C2, Cell Signaling Technology); V5 (A00623-100, GeneScripts); phosphotyrosine (4G10 Platinum, anti-phosphotyrosine 05-1050X, Millipore); total ROS1 (3266S, clone 69D6, Cell Signaling Technology); phospho-ROS1 (Tyr2274) (3078S, Cell Signaling Technology); and β-actin clone 13E5 (4970S, Cell Signaling Technology).

Intracranial Injection

Female NSG mice (4–6 months old) were anesthetized with ketamine/xylazine and treated with a preoperative dose of buprenorphine prior to craniotomy, after which 500,000 mouse *Bcan–Ntrk1* glioma cells harboring the TRKA^{G670C} substitution were delivered per animal via stereotactic intracranial injection targeting the neurogenic region of the right lateral ventricle. One week later, brain MRI was performed using a Bruker 4.7T Biospec scanner by the Animal Imaging Core Facility at MSKCC. Images were visualized with the online miniPACS software. Mice were then randomized based on tumor size (calculated using ImageJ software) in vehicle ($n = 3$) and cabozantinib ($n = 4$) groups. Animals were treated with vehicle or cabozantinib daily (100 mg/mL) via oral gavage. At day 7 of treatment, a second MRI was performed using the same scanner. Tumor size was quantified in both groups, and data were then analyzed using GraphPad 8.1.2. Treatments were continued until the mice were sacrificed to obtain survival curves. Mouse experiments were approved by the MSKCC Institutional Animal Care and Use Committee.

Patient-Derived Primary Cell Lines

The entrectinib-resistant *LMNA–NTRK1*, TRKA^{G595R} colorectal cancer cell line was obtained from A. Bardelli. The *LMNA–NTRK1*, TRKA$^{G595R/G667C}$ cell line was established following chronic exposure of the *LMNA–NTRK1*, TRKA^{G595R} to increasing concentrations of repotrectinib (ranging from 1 to 500 nmol/L) for 5 months. Cell lines were plated on Petri dishes and cultured in DMEM Nutrient Mixture F-12 + 10% fetal bovine serum and 1% antibiotics.

Xenografts and PDX Studies

Xenografts derived from the *LMNA–NTRK1*, TRKA^{G595R}/TRKA^{G667C} colorectal cancer primary cell line were generated by injecting 5 million cells into the flank of 6-week-old NSG female mice. When tumors reached 100 mm^3 in size, the mice were randomized and dosed orally with vehicle, repotrectinib (100 mg/kg daily 5 days per week), or cabozantinib (100 mg/kg daily, 5 days per week). PDXs derived from Patient 1 were randomized and dosed orally with vehicle, selitrectinib (100 mg/kg twice daily, 5 days per week) or cabozantinib (100 mg/kg daily, 5 days per week). PDXs derived from Patient 3 were randomized and dosed orally with vehicle, selitrectinib (100 mg/kg twice daily, 5 days per week), repotrectinib (100 mg/kg daily, 5 days per week), or cabozantinib (100 mg/kg daily, 5 days per week). Tumors were measured twice weekly using calipers, and tumor volume was calculated using the formula length × width^2 × 0.52. Body weight was also assessed twice weekly. Mice were cared for in accordance with guidelines approved by the MSKCC Institutional Animal Care and Use Committee and Research Animal Resource Center. Six to eight mice per group were included in each experiment.

Authors' Disclosures

S. Kannan reports he is Founder of Sinopsee Therapeutics and Aplomex; neither company has any conflict with current work. A.M. Schram reports grants from NIH T32 CA009207 and grants from ASCO Young Investigator Award during the conduct of the study. E. Toska has received honoraria from Astrazeneca for invited lectures. S. Arena reports personal fees from MSD Italia outside the submitted work. N. Vasan reports other from Novartis, non-financial support from Petra Pharmaceuticals, non-financial support from Volastra Therapeutics, and other from Heligenics, Inc. outside the submitted work. M.F. Berger reports personal fees from Roche and grants from Grail outside the submitted work. Y. Liao reports grants from NIH/NCI during the conduct of the study. U. Rix reports grants from NIH/NCI during the conduct of the study; in addition, U. Rix has a patent for U.S. Provisional Application No. 61/952,757 pending. S. Misale reports personal fees from Boehringer-Ingelheim outside the submitted work. B.S. Taylor reports grants from Genentech, Inc., personal fees from Boehringer-Ingelheim, and personal fees from Loxo Oncology at Lilly outside the submitted work. A. Bardelli reports non-financial support from Horizon Discovery, grants from Neophore, non-financial support from Biocartis, personal fees from Roche, and personal fees from Illumina outside the submitted work. J.F. Hechtman reports grants from Bayer, personal fees from WebMD, personal fees from ESMO/Oncology Pro, personal fees from Axiom Healthcare Strategies, and personal fees from Bayer outside the submitted work. D.M. Hyman reports grants from Bayer during the conduct of the study; other from Lilly/Loxo Oncology outside the submitted work. C.S. Verma reports grants from MSD International and grants from Ipsen outside the submitted work; and C.S. Verma is the founder of Sinopsee Therapeutics and Aplomex; neither company has any conflict with

the current work. A. Drilon reports other from Loxo/Bayer/Lilly, other from Ignyta/Genentech/Roche, and other from TP Therapeutics during the conduct of the study; other from Takeda/Ariad/Millennium, other from AstraZeneca, other from Pfizer, other from Blueprint Medicines, other from Helsinn, other from Beigene, other from BergenBio, other from Hengrui, other from Exelixis, other from Tyra, other from Verastem, other from MORE Health, other from Abbvie, other from 14ner/Elevation Oncology, other from Remedica , other from ArcherDX, other from Monopteros, other from Novartis, other from EMD Serono, and other from Melendi outside the submitted work; and associated research paid to institution: Pfizer, Exelixis, GlaxoSmithKline, Teva, Taiho, PharmaMar; research: Foundation Medicine; royalties: Wolters Kluwer, OTHER: Merck, Puma, Merus, Boehringer-Ingelheim; CME honoraria: Medscape, OncLive, PeerVoice, Physicians Education Resources, Targeted Oncology, Research to Practice, Axis, Peerview Institute, Paradigm Medical Communications, WebMD, MJH Life Sciences. M. Scaltriti reports grants from Puma Biotechnology, grants from Targimmune, grants from AstraZeneca, grants and personal fees from Menarini Ricerche, grants and personal fees from Daiichi-Sankyo, grants from BD Therapeutics, grants from Immunomedics, and personal fees from Bioscience Institute during the conduct of the study. No disclosures were reported by the other authors..

Authors' Contributions

E. Cocco: Conceptualization, supervision, funding acquisition, investigation, writing-original draft, project administration, writing-review and editing. **J.E. Lee:** Conceptualization, data curation, methodology, writing-original draft. **S. Kannan:** Data curation, software, formal analysis, investigation, visualization. **A.M. Schram:** Data curation, formal analysis, validation, investigation. **H.H. Won:** Data curation, software, formal analysis. **S. Shifman:** Validation, investigation, methodology. **A. Kulick:** Data curation, methodology. **L. Baldino:** Data curation, validation, methodology, data curation, validation, methodology. **E. Toska:** Supervision, investigation. **A. Arruabarrena-Aristorena:** Investigation, methodology, investigation, methodology. **S. Kittane:** Data curation, validation, investigation, methodology. **F. Wu:** Validation, methodology. **Y. Cai:** Data curation, formal analysis, validation, methodology. **S. Arena:** Data curation, validation, methodology. **B. Mussolin:** Data curation, software, validation, visualization, methodology. **R. Kannan:** Resources, data curation, software, formal analysis, methodology. **N. Vasan:** Data curation, validation, investigation, methodology. **A.N. Gorelick:** Data curation, software, validation, investigation, visualization, methodology. **M.F. Berger:** Resources, software, formal analysis, methodology. **O. Novoplansky:** Supervision, validation, investigation, methodology. **S. Jagadeeshan:** Resources, supervision, validation, investigation, methodology. **Y. Liao:** Data curation, validation, investigation, methodology. **U. Rix:** Resources, supervision, methodology. **S. Misale:** Data curation, supervision, validation, investigation, methodology. **B.S. Taylor:** Data curation, software, supervision, visualization, methodology. **A. Bardelli:** Conceptualization, resources, software, formal analysis, supervision, investigation, visualization, methodology, writing-original draft, writing-review and editing. **J.F. Hechtman:** Conceptualization, data curation, supervision, validation, investigation, methodology, writing-review and editing. **D.M. Hyman:** Conceptualization, resources, data curation, formal analysis, supervision, funding acquisition, writing-original draft, writing-review and editing. **M. Elkabets:** Conceptualization, resources, data curation, supervision, funding acquisition, investigation, methodology, writing-original draft, project administration, writing-review and editing. **E. de Stanchina:** Data curation, software, supervision, visualization, methodology. **C.S. Verma:** Conceptualization, data curation, software, formal analysis, supervision, investigation, visualization, methodology, writing-original draft, writing-review and editing. **A. Ventura:** Conceptualization, supervision, validation, investigation, methodology, writing-review and editing. **A. Drilon:** Conceptualization, resources, data curation, formal analysis, supervision, funding acquisition, validation, investigation, writing-original draft, writing-review and editing. **M. Scaltriti:** Conceptualization, resources, data curation, formal analysis, supervision, funding acquisition, validation, investigation, methodology, writing-original draft, project administration, writing-review and editing.

Acknowledgments

This study was funded by the National Cancer Institute (NCI) under MSK Cancer Center Support Grant/Core Grant P30 CA008748 and R01CA226864 (to M. Scaltriti and A. Drilon). This work was also funded by the Cycle for Survival (to A. Drilon), Nonna's Garden Foundation (A. Drilon, A.M. Schram, D.M. Hyman, M. Scaltriti), NIH T32 CA009207, and ASCO Young Investigator Award (A.M. Schram). Work by J.E. Lee and A. Ventura was funded by the Geoffrey Beene Cancer Research Foundation, STARR Foundation, and Pershing Square Cancer Research Foundation. E. Cocco is a recipient of an MSK Society Scholars Prize and of an NIH-sponsored Translational Research in Oncology Training fellowship (5 T32 CA160001-08). We thank A*STAR (IAF-PP grant H18/01/a0/015) and the National Supercomputing Centre, Singapore, for support. The work was also supported by The United States–Israel Binational Science Foundation (2017323, to M. Elkabets and M. Scaltriti). The work of Y. Liao and U. Rix was funded by R01CA181746 (to U. Rix). The research leading to these results has received funding from Fondazione AIRC under the 5 per Mille 2018 ID. 21091 program (PI, A. Bardelli); AIRC IG 2018 ID. 21923 project (PI, A. Bardelli); Fondazione Piemontese per la Ricerca sul Cancro-ONLUS 5 per Mille 2014 e 2015 Ministero della Salute (A. Bardelli); and AIRC under MFAG 2017 ID. 20236 project (PI, S. Arena).

The costs of publication of this article were defrayed in part by the payment of page charges. This article must therefore be hereby marked *advertisement* in accordance with 18 U.S.C. Section 1734 solely to indicate this fact.

Received May 1, 2020; revised August 26, 2020; accepted September 28, 2020; published first October 1, 2020.

REFERENCES

1. Recondo G, Facchinetti F, Olaussen KA, Besse B, Friboulet L. Making the first move in EGFR-driven or ALK-driven NSCLC: first-generation or next-generation TKI? Nat Rev Clin Oncol 2018;15:694–708.
2. Lin JJ, Riely GJ, Shaw AT. Targeting ALK: precision medicine takes on drug resistance. Cancer Discov 2017;7:137–55.
3. Lin JJ, Shaw AT. Recent advances in targeting ROS1 in lung cancer. J Thorac Oncol 2017;12:1611–25.
4. Schram AM, Chang MT, Jonsson P, Drilon A. Fusions in solid tumours: diagnostic strategies, targeted therapy, and acquired resistance. Nat Rev Clin Oncol 2017;14:735–48.
5. Vasan N, Baselga J, Hyman DM. A view on drug resistance in cancer. Nature 2019;575:299–309.
6. Cocco E, Schram AM, Kulick A, Misale S, Won HH, Yaeger R, et al. Resistance to TRK inhibition mediated by convergent MAPK pathway activation. Nat Med 2019;25:1422–7.
7. Cocco E, Scaltriti M, Drilon A. NTRK fusion-positive cancers and TRK inhibitor therapy. Nat Rev Clin Oncol 2018;15:731–47.
8. Drilon A, Laetsch TW, Kummar S, DuBois SG, Lassen UN, Demetri GD, et al. Efficacy of larotrectinib in TRK fusion-positive cancers in adults and children. N Engl J Med 2018;378:731–9.
9. Drilon A, Siena S, Ou SI, Patel M, Ahn MJ, Lee J, et al. Safety and antitumor activity of the multitargeted pan-TRK, ROS1, and ALK inhibitor entrectinib: combined results from two phase I trials (ALKA-372-001 and STARTRK-1). Cancer Discov 2017;7:400–9.

10. Demetri GD, Paz-Ares L, Farago AF, Liu SV, Chawla SP, Tosi D, et al. LBA17. Efficacy and safety of entrectinib in patients with NTRK fusion-positive (NTRK-fp) tumors: pooled analysis of STARTRK-2, STARTRK-1 and ALKA-372-001. Ann Oncol 2018;29 Suppl 8:VIII713.
11. Drilon A, Li G, Dogan S, Gounder M, Shen R, Arcila M, et al. What hides behind the MASC: clinical response and acquired resistance to entrectinib after ETV6-NTRK3 identification in a mammary analogue secretory carcinoma (MASC). Ann Oncol 2016;27:920–6.
12. Russo M, Misale S, Wei G, Siravegna G, Crisafulli G, Lazzari L, et al. Acquired resistance to the TRK inhibitor entrectinib in colorectal cancer. Cancer Discov 2016;6:36–44.
13. Drilon A, Nagasubramanian R, Blake JF, Ku N, Tuch BB, Ebata K, et al. A next-generation TRK kinase inhibitor overcomes acquired resistance to prior TRK kinase inhibition in patients with TRK fusion-positive solid tumors. Cancer Discov 2017;7:963–72.
14. Drilon A, Ou SI, Cho BC, Kim DW, Lee J, Lin JJ, et al. Repotrectinib (TPX-0005) is a next-generation ROS1/TRK/ALK inhibitor that potently inhibits ROS1/TRK/ALK solvent-front mutations. Cancer Discov 2018;8:1227–36.
15. Modi V, Dunbrack RL Jr. Defining a new nomenclature for the structures of active and inactive kinases. Proc Natl Acad Sci U S A 2019;116:6818–27.
16. Zhang J, Yang PL, Gray NS. Targeting cancer with small molecule kinase inhibitors. Nat Rev Cancer 2009;9:28–39.
17. Vijayan RS, He P, Modi V, Duong-Ly KC, Ma H, Peterson JR, et al. Conformational analysis of the DFG-out kinase motif and biochemical profiling of structurally validated type II inhibitors. J Med Chem 2015;58:466–79.
18. Bagal SK, Andrews M, Bechle BM, Bian J, Bilsland J, Blakemore DC, et al. Discovery of potent, selective, and peripherally restricted pan-Trk kinase inhibitors for the treatment of pain. J Med Chem 2018;61:6779–800.
19. Fuse MJ, Okada K, Oh-Hara T, Ogura H, Fujita N, Katayama R. Mechanisms of resistance to NTRK inhibitors and therapeutic strategies in NTRK1-rearranged cancers. Mol Cancer Ther 2017;16:2130–43.
20. Konicek BW, Capen AR, Credille KM, Ebert PJ, Falcon BL, Heady GL, et al. Merestinib (LY2801653) inhibits neurotrophic receptor kinase (NTRK) and suppresses growth of NTRK fusion bearing tumors. Oncotarget 2018;9:13796–806.
21. Shen B, Wu F, Ye J, Liang R, Wang R, Yu R, et al. Crizotinib-resistant MET mutations in gastric cancer patients are sensitive to type II tyrosine kinase inhibitors. Future Oncol 2019;15:2585–93.
22. Smith CC, Lin K, Stecula A, Sali A, Shah NP. FLT3 D835 mutations confer differential resistance to type II FLT3 inhibitors. Leukemia 2015;29:2390–2.
23. Hari SB, Merritt EA, Maly DJ. Sequence determinants of a specific inactive protein kinase conformation. Chem Biol 2013;20:806–15.
24. Drilon A, Jenkins C, Iyer S, Schoenfeld A, Keddy C, Davare MA. ROS1-dependent cancers - biology, diagnostics and therapeutics. Nat Rev Clin Oncol 2020 Aug 6 [Epub ahead of print].
25. Cook PJ, Thomas R, Kannan R, de Leon ES, Drilon A, Rosenblum MK, et al. Somatic chromosomal engineering identifies BCAN-NTRK1 as a potent glioma driver and therapeutic target. Nat Commun 2017;8:15987.
26. Ciccarese C, Iacovelli R, Mosillo C, Tortora G. Exceptional response to cabozantinib of rapidly evolving brain metastases of renal cell carcinoma: a case report and review of the literature. Clin Genitourin Cancer 2018;16:e1069–e71.
27. Lovera S, Morando M, Pucheta-Martinez E, Martinez-Torrecuadrada JL, Saladino G, Gervasio FL. Towards a molecular understanding of the link between imatinib resistance and kinase conformational dynamics. PLoS Comput Biol 2015;11:e1004578.
28. Brown BP, Zhang YK, Westover D, Yan Y, Qiao H, Huang V, et al. On-target resistance to the mutant-selective EGFR inhibitor osimertinib can develop in an allele-specific manner dependent on the original EGFR-activating mutation. Clin Cancer Res 2019;25:3341–51.
29. Bahcall M, Sim T, Paweletz CP, Patel JD, Alden RS, Kuang Y, et al. Acquired METD1228V mutation and resistance to MET inhibition in lung cancer. Cancer Discov 2016;6:1334–41.
30. Laine E, Auclair C, Tchertanov L. Allosteric communication across the native and mutated KIT receptor tyrosine kinase. PLoS Comput Biol 2012;8:e1002661.
31. Nakaoku T, Kohno T, Araki M, Niho S, Chauhan R, Knowles PP, et al. A secondary RET mutation in the activation loop conferring resistance to vandetanib. Nat Commun 2018;9:625.
32. Drilon A, Somwar R, Wagner JP, Vellore NA, Eide CA, Zabriskie MS, et al. A novel crizotinib-resistant solvent-front mutation responsive to cabozantinib therapy in a patient with ROS1-rearranged lung cancer. Clin Cancer Res 2016;22:2351–8.
33. Oliveres H, Pineda E, Maurel J. MET inhibitors in cancer: pitfalls and challenges. Expert Opin Investig Drugs 2020;29:73–85.
34. Sumi NJ, Ctortecka C, Hu Q, Bryant AT, Fang B, Remsing Rix LL, et al. Divergent polypharmacology-driven cellular activity of structurally similar multi-kinase inhibitors through cumulative effects on individual targets. Cell Chem Biol 2019;26:1240–52.
35. Ferguson FM, Gray NS. Kinase inhibitors: the road ahead. Nat Rev Drug Discov 2018;17:353–77.
36. Ikemura S, Yasuda H, Matsumoto S, Kamada M, Hamamoto J, Masuzawa K, et al. Molecular dynamics simulation-guided drug sensitivity prediction for lung cancer with rare EGFR mutations. Proc Natl Acad Sci U S A 2019;116:10025–30.
37. Zehir A, Benayed R, Shah RH, Syed A, Middha S, Kim HR, et al. Mutational landscape of metastatic cancer revealed from prospective clinical sequencing of 10,000 patients. Nat Med 2017;23:703–13.
38. Cheng DT, Mitchell TN, Zehir A, Shah RH, Benayed R, Syed A, et al. Memorial sloan kettering-integrated mutation profiling of actionable cancer targets (MSK-IMPACT): a hybridization capture-based next-generation sequencing clinical assay for solid tumor molecular oncology. J Mol Diagn 2015;17:251–64.
39. Chang MT, Asthana S, Gao SP, Lee BH, Chapman JS, Kandoth C, et al. Identifying recurrent mutations in cancer reveals widespread lineage diversity and mutational specificity. Nat Biotechnol 2016;34:155–63.
40. Chang MT, Bhattarai TS, Schram AM, Bielski CM, Donoghue MTA, Jonsson P, et al. Accelerating discovery of functional mutant alleles in cancer. Cancer Discov 2018;8:174–83.
41. Kaminski GA, Friesner RA, Tirado-Rives J, Jorgensen WL. Evaluation and reparametrization of the OPLS-AA force field for proteins via comparison with accurate quantum chemical calculations on peptides. J Phys Chem B 2001;105:6474–87.
42. Friesner RA, Banks JL, Murphy RB, Halgren TA, Klicic JJ, Mainz DT, et al. Glide: a new approach for rapid, accurate docking and scoring. 1. Method and assessment of docking accuracy. J Med Chem 2004;47:1739–49.
43. Case DA, Ben-Shalom IY, Brozell SR, Cerutti DS, Cheatham TE, Cruzeiro VWD, et al. AMBER 2018. San Francisco: University of California, San Francisco; 2018.
44. Maier JA, Martinez C, Kasavajhala K, Wickstrom L, Hauser KE, Simmerling C. ff14SB: improving the accuracy of protein side chain and backbone parameters from ff99SB. J Chem Theory Comput 2015;11:3696–713.
45. Wang J, Wolf RM, Caldwell JW, Kollman PA, Case DA. Development and testing of a general amber force field. J Comput Chem 2004;25:1157–74.
46. Jorgensen WL, Chandrasekhar J, Madura JD, Impey RW, Klein ML. Comparison of simple potential functions for simulating liquid water. J Chem Phys 1983;79:926–35.
47. 3rd Current Topics in Gastroenterology Symposium. Sandpiper, Florida, October 31-November 2, 1993. Proceedings. Scand J Gastroenterol Suppl 1995;208:1–148.
48. Miyamoto S, Kollman PA. Settle: an analytical version of the SHAKE and RATTLE algorithm for rigid water models. J Comput Chem 1992;13:952–62.
49. Humphrey W, Dalke A, Schulten K. VMD: visual molecular dynamics. J Mol Graph 1996;14:33–8, 27–8.
50. DeLano WL. The PyMOL molecular graphics system. San Carlos (CA): De Lano Scientific; 2002.